Agile Maneuvering for Fin-Actuated Underwater Vehicles

Kristi A. Morgansen, Timothy M. La Fond, and Jennifer X. Zhang

Abstract— **Underwater locomotion and propulsion for underwater vehicles provide rich applications for the development of control methods for nonlinear systems and underactuated mechanical systems. In the work here, the tasks of modeling and control for agile gait generation for robots built with fin propulsive and maneuvering surfaces are considered. Previous work for such bioinspired devices has shown that simplified models with quasistatic lift and drag can be used to construct trajectory tracking controls for forward and turning motions that strongly resemble biomimetic motions. Here we will evaluate the use of such models for agile maneuverability by comparing biomimetic snap turn data from experiment with simulation data from the model. Such results can then be used to indicate approaches for more exact theoretical investigation of bioinspired control for agile maneuverability.**

I. Introduction

The development of autonomous underwater vehicles has progressed quite significantly in the past decade due in large part to the increasing interest in unmanned underwater surveillance and monitoring. Of particular interest are regions of the underwater environment which are cluttered and dynamic. An approach that has shown promise for design of vehicles suitable to such environments is to draw from nature, both vehicle morphology and methods of locomotion. The study of underwater locomotion has long been a subject of interest to the biological community [1], [2], [3], [4], [5], [6]. The robotics and engineering communities have been inspired by this research to construct mechanisms that mimic the behavior of swimming lifeforms. The appeal of such designs lies in the potential for greater agility and maneuverability at low speeds, decreased hydrodynamic noise from cavitation, and decreased drag. A large portion of the work that has been performed relative to swimming vehicles has focused on the task of forward locomotion [7], [8], [9], [10], [11], [12], [13]. Further most of these approaches have been either empirical, focusing on issues of propulsive efficiency and fluid flow effects, or kinematic where the complexities of explicit fluid force calculations can be side-stepped.

Here we will explore the agile maneuverability of a fish-like underwater vehicle. Specifically, we will consider the production of fast turns as observed in nature. Some prior work has considered such motions [14], [15], and has approached the problem through the use of biomimicry– duplicating observed behaviors from nature as closely as possible in engineered systems. Our work here is similar in terms of experimental implementation, however, our end goal is quite different. In earlier work, we have shown how dynamics based models that incorporate lift, drag and added mass effects can be used for analytical controller design for fin-actuated underwater vehicles [9], [10]. Forward and slow turning modes of locomotion were generated by applying generic techniques for control of nonlinear system rather than by appealing to kinematic results from observations of nature. Such results are powerful in that a range of questions can be addressed with analytical models that cannot be with empirical ones, and behaviors not observed in nature may be of benefit in engineered systems.

The work in this paper specifically addresses the usefulness of our earlier model for purposes of agile maneuverability. We will demonstrate the construction of controls that generate snap turns in experiment on our robot and will then show the results of applying these same controls to our models. The end result will be some qualitative agreement, but a need for refinement of the model. The paper is organized as follows. In Section II, the analytical model is presented. In Section III, the experimental apparatus is discussed. The construction of snap turn controls is given in Section IV. Experimental and simulation results are given in Section V. Directions for future work are discussed in Section VI.

II. System Model

We approximate the carangiform style of locomotion using a fully submersed three-link mechanism with two actuated joints. The first link functions as the "body" and is roughly two-thirds of the length of the entire robot. The "tail" of the robot is formed by the second and third links (see Fig. 1). Our mechanism is a reasonably general planar approximation to carangiform locomotion, and therefore small modifications of this model should have general utility in the analysis of carangiform swimming. In particular, the methods and techniques presented here are applicable to a tail with any degree of articulation or even full flexibility.

We will assume that the water is inviscid, irrotational and incompressible as well as infinite in domain. We neglect three-dimensional fluid effects and assume that we can restrict our attention to a plane perpendicular to the direction of gravity (and therefore neglect the effects of gravity and of buoyancy). As we are not modeling the state of the fluid, change in fluid energy is accounted for by assuming an apparent increase in the mass of the object, termed added mass, in the direction the object is accelerated. The forces incorporated into the system model here are then added mass, lift, and drag (see Fig. 1). However, we emphasize that the control methods to be discussed admit the use of a much

This work was supported in part by NSF grant CMS-0238461 and in part by the University of Washington NASA Space Grant. K.A. Morgansen, T.M. La Fond, and J.X. Zhang are with the Department of Aeronautics and Astronautics, University of Washington, Seattle, WA 98195, USA {morgansn,tmlf,jxzhang}@u.washington.edu

broader range of external forces than those considered in this work.

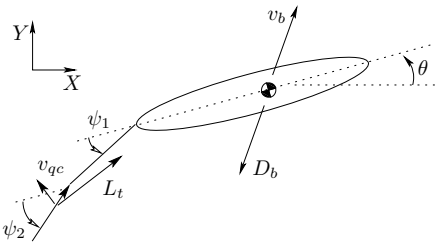

Fig. 1. Free body diagram of carangiform robot.

As a mechanical system, our robot has a configuration space given by $Q = \mathbb{S}^1 \times \mathbb{S}^1 \times SE(2)$. We denote the coordinates of $q \in Q$ by $q = [\psi_1, \psi_2, x_1, x_2, \theta]$ where the body link coordinates $[x_1, x_2, \theta]$ are the coordinates of the origin of a body-fixed coordinate frame located at the center of mass of the body link, measured relative to an inertial reference frame. The angle ψ_1 is measured relative to the longitudinal axis of the body link, and ψ_2 is measured relative to ψ_1. The manifold $SE(2)$, in which the states $[x_1, x_2, \theta]$ evolve, is a Lie group generically denoted by G with Lie algebra $\mathfrak{g}$, and these states are referred to as the *group* states.

The configuration of a body-fixed coordinate frame located at the body link center of mass, measured relative to an inertial frame and denoted by $g \in G$, can be represented using homogeneous matrix notation as $g = \begin{bmatrix} R & x \\ 0 & 1 \end{bmatrix}$, where $x = [x_1, x_2]^T$ and $R \in SO(1)$, denotes the orientation of the body link relative to an inertial frame. The translational and angular velocities are denoted by the vector $[\dot{x}_1, \dot{x}_2]^T = V \in \mathbb{R}^2$ and the scalar $\omega \in \mathbb{R}$. In this notation, the velocity of the body link is then given by

$$\begin{aligned} \dot{R} &= R\widehat{\omega} \\ \dot{x} &= RV \end{aligned} \tag{1}$$

where $\widehat{\omega} = \begin{bmatrix} 0 & -\omega \\ \omega & 0 \end{bmatrix}$.

For a rigid body in a fluid, the mass matrix (material plus added mass) is constant relative to such a body-fixed frame as long as we assume that the added mass of a particular link is independent of all other links. In particular, for a planar flat plate of length l and height h in an ideal fluid, the added mass and inertia values are given by

$$m_{x_1} = 0,\ m_{x_2} = \rho\pi \left(\frac{l}{2}\right)^2 h,\ m_\theta = 2\pi\rho \left(\frac{l}{4}\right)^4 h$$

with x_1 measured along the length of the plate. The corresponding mass matrix is

$$M = \begin{bmatrix} m_{mat} + m_{x_1} & 0 & 0 \\ 0 & m_{mat} + m_{x_2} & 0 \\ 0 & 0 & J_{mat} + m_\theta \end{bmatrix},$$

where m_{mat} and J_{mat} are the link material mass and inertia.

Assuming no potential energy is present in the system, the Lagrangian is then given by

$$L(q, \dot{q}) = \frac{1}{2} \sum_{i=1}^{k} V_i^T M_i V_i = \frac{1}{2} \dot{q}^T M(q) \dot{q},$$

where V_i and M_i are functions of the system states $q = [r^T, g^T]^T$ and $\dot{q} = [\dot{r}^T, \dot{g}^T]^T$. The mass matrix for an immersed mechanical system will change based on the joint angles r, but will not depend on the group states g. Therefore, we can rewrite the Lagrangian using the body-fixed velocity of the group states $\xi = g^{-1}\dot{g}$ to give the reduced Lagrangian for the system is given by

$$l(r, \dot{r}, \xi) = L(r, e, \dot{r}, \xi) = \frac{1}{2} \begin{bmatrix} \dot{r} \\ \xi \end{bmatrix}^T M(r) \begin{bmatrix} \dot{r} \\ \xi \end{bmatrix},$$

where $e \in G$ is the group identity element and $M(r) = M(r, e)$ is the reduced mass matrix.

The dynamics corresponding to the reduced Lagrangian are given by the Euler-Poincaré equations,

$$\frac{d}{dt}\frac{\partial l}{\partial \dot{r}} - \frac{\partial l}{\partial r} = f^r \tag{2a}$$

$$\frac{d}{dt}\frac{\partial l}{\partial \xi} = ad^*_\xi \frac{\partial l}{\partial \xi} + f^\xi \tag{2b}$$

together with the reconstruction equation,

$$\dot{g} = g\,\xi, \tag{3}$$

where f^r, f^ξ are external forces on the system in body coordinates, and ad^*_ξ is the dual to the Lie bracket $ad_\xi \eta = [\xi, \eta]$. While this structure may seem overly abstract, its usefulness lies in the fact that it completely describes the generalization for arbitrary number of links in the tail, is valid regardless of the space in which the vehicle operates (planar or 3D), the form of external forces such as lift and drag does not affect the system structure, and additional forces can be added in exactly the same way. Therefore the results we derive here based on this structure are applicable to any shape-actuated underwater vehicle including those with a flexible tail.

III. Experimental Apparatus

The physical device being used in the experimental work discussed here is shown in Fig. 2. The first two components

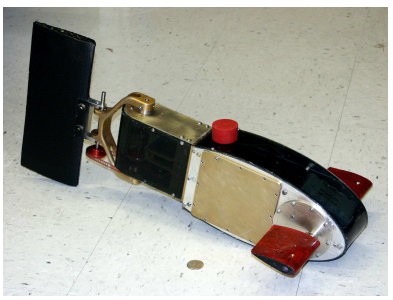

Fig. 2. Side view of autonomous fi n-actuated underwater robot.

form the body of the robot and are composed of an aluminum frame and a combination of aluminum and acrylic panels.

The first compartment contains the microcontroller (Axiom PB-0555 microcontroller board with Motorola MPC555 PowerPC microprocessor), sensing devices, pectoral fin servo motors, and batteries. The second compartment contains the servo motors for the two tail links. The tail is composed of a wishbone shaped "peduncle" region and a rectangular flat plate for the caudal fin. The pectoral fins are actuated with Airtronics 94091Z super microlite servo motors, and the tail joints are actuated with a Hitec HS-5925MG high speed and HS-5945MG high-torque micro servo motors. The pectoral fin motors are capable of 23 oz-in torque at 6V, and the tail servos are respectively capable of 120 oz-in and 180 oz-in torque at 6V.

Physical dimensions of the robot are shown in Fig. 3. The overall weight is approximately 2kg. The centers of

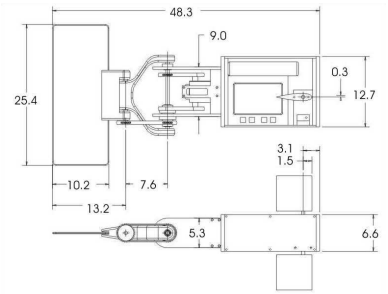

Fig. 3. Robot design schematic (measurements in cm).

buoyancy and gravity are engineered to be co-linear (but not coincident) along the body x_3 axis using externally applied styrofoam and steel shims for buoyancy and weight, respectively. The pectoral fins are composed of dense styrofoam and fiberglass and are located forward and above the center of mass. The fins are NACA 0021 airfoils with chord length $6.9cm$ and span $7.8cm$. The lift force generated by a fin is assumed to act at the quarter chord point of the fin.

The measurement of angular and position data of the robots motion in the plane, as presented here, were collected using image tracking from a camera suspended over the experimental tank. The camera is a Logitech QuickCam 4000 running at 30fps with resolution of 320x240 pixels. The video is captured with a Pentium 4 PC running Linux and moTV. To calibrate the image a grid was placed on the surface of the water and an image was taken. Point pairs were then calibrated using Tsai's camera calibration method. A black and white image of the letter 'T' was attached to the top of the robot to assist in tracking.

IV. Biomimetic Modeling of Snap Turns

As a first step in evaluating the above model for use in agile maneuvering, we will address the ability of the model to replicate motions such as fast starts and snap turns. In order to determine the angular values necessary to generate such a motion, we draw from experimental results in live fish experiments [4]. A sample of such an experiment is shown in Fig. 4 where each line represents the curve of the backbone of a goldfish during a snap turn maneuver. The lines are separated in time by 0.04s.

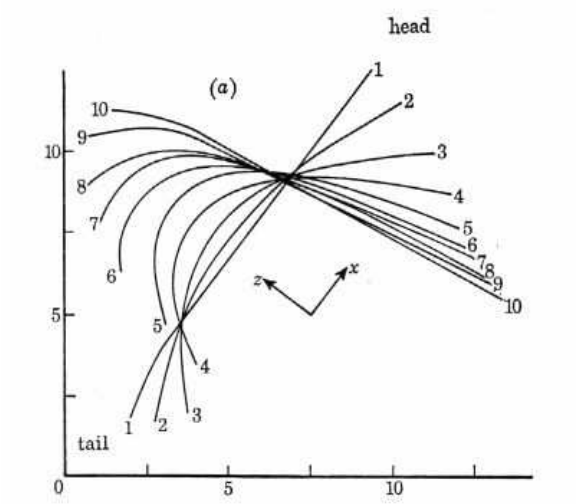

Fig. 4. Tracing of backbone position of a goldfi sh making a snap turn [4]. Time between each frame is 0.04s.

In order to map these curves to achievable configurations of the robot, the following steps were performed. Each line was digitally captured and reoriented such that the head end of the curve had zero orientation and scaled to have the same length as the robot. A least squares fit was then performed for each line segment of the robot relative to a corresponding length segment of the curve. Given the joint angles for each of the ten segments, a fifth order polynomial is fit to the data to create smooth functions of time for the full motion. The resulting curves for the two joints are shown in Fig. 5. Clearly this method of constructing joint angles in order to

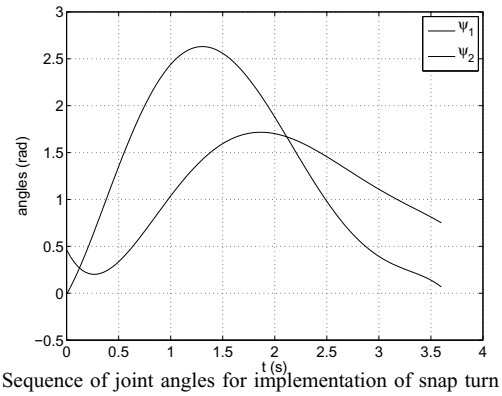

Fig. 5. Sequence of joint angles for implementation of snap turn on three link robot. The plot shows the joint angles as functions of time through the motion.

produce a snap turn is somewhat crude and could easily be refined as in [14], [15]. However, our interest here is not to recreate precisely what happens with a fish but to explore the capabilities of our model relative to the experimental apparatus.

V. Results

The angular functions determined in the preceding section were applied directly to the fish robot both as they were determined and also with scaled amplitude. The intent behind the scaling was to verify that the essential features of a snap

turn were captured by the derivation process. The results for a set of four experiments are shown in Fig. 6. As desired,

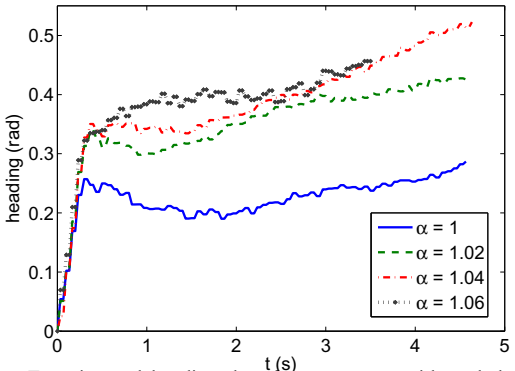

Fig. 6. Experimental heading data for snap turns with scaled amplitude from $\alpha = 1.0$ through 1.06.

the magnitude of the turn increased as the amplitude of the joint motions was increased. The point on the body at which the angular measurements was made was roughly over the center of mass of the body. Given that the data was collected with an overhead camera, the relative amount of noise in the data is quite reasonable.

A corresponding plot of simulation results for the corresponding angles and scalings is shown in Fig. 7. Clearly,

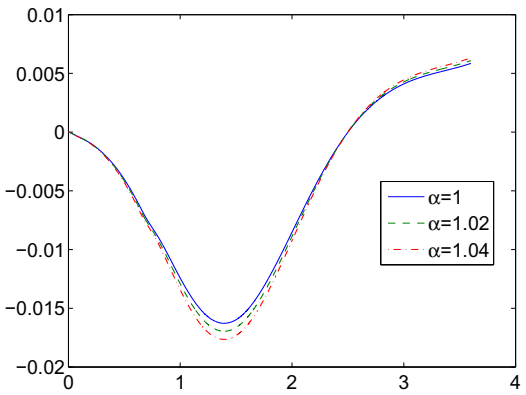

Fig. 7. Simulation heading data for snap turns with scaled amplitude from $\alpha = 1.0$ through 1.06.

the model has not performed as well in producing snap turns as the experimental apparatus. However, the general qualitative shape of the motion is somewhat similar to that of the experimental results. Specifically, the heading of the robot swings wide as the body coils, then returns to a smaller angle as the body straightens out. A number of likely reasons for the discrepancies can be considered, based on the approximations that were made when calculating the forces applied to the system. First, the added mass of the system was calculated as the sum of the added masses of the individual links, taken as if the other links were not present. This approximation is not unreasonable when the system is in an extended configuration, but errors grow quickly when such an approximation is used for highly deformed shapes such as those that occur with the early stages of a snap turn. Second, the coefficients of lift and drag have been assumed static functions of angle of attack and rotational velocity. This approximation is reasonable when flow conditions are near steady and the system is fully extended. In the situation of a snap turn, as the flow is unsteady and the body is not in an extended configuration, this approximation loses validity. Further, the functions for the coefficients of lift and drag have been chosen more for their amenability to analysis than for precise reflection of realistic flow conditions as such realistic data is not available for the type of operation and system under consideration.

VI. Conclusion

The work in this paper has addressed the construction of controls for snap turn motions in a fin-actuated underwater vehicle and the comparison of these controls both in simulation and in a dynamics-based model. While the experimental results performed quite well, the simulation results were not a good match. Most likely some thought needs to be given to refinement of the fluid forces being used in the model. However, the qualitative behavior of the simulated system is not entirely unreasonable and suggests that with refinement the model may be suitable without the addition of unsteady effects or the need for empirical modeling.

References

[1] S. Childress, *Mechanics of Swimming and Flying*. Cambridge: Cambridge University Press, 1981.

[2] J. Lighthill, *Mathematical Biofluiddynamics*. Philadelphia: SIAM, 1975.

[3] J. Newman and T. Wu, "Hydrodynamical aspects of fish swimming," in *Swimming and Flying in Nature, Vol 2.*, T. Wu, C. Brokaw, and C. Brennen, Eds. New York: Plenum Press, 1975, pp. 615–34.

[4] D. Weihs, "A hydrodynamical analysis of fish turning manoeuvres," *Proc. R. Soc. Lond. B*, vol. 182, pp. 59–72, 1972.

[5] I. Spierts and J. van Leeuwen, "Kinematics and muscle dynamics of C- and S-starts of carp (cyprinus carpio L.)," *J. Exp. Biology*, vol. 202, pp. 393–406, 1999.

[6] P. Domenici and R. Blake, "The kinematics and performance of fish fast-start swimming," *J. Exp. Biology*, vol. 200, pp. 1165–1178, 1997.

[7] M. Triantafyllou and G. Triantafyllou, "An efficient swimming machine," *Scientific American*, pp. 64–70, Mar. 1995.

[8] D. Barrett, M. Grosenbaugh, and M. Triantafyllou, "The optimal control of a flexible hull robotic undersea vehicle propelled by an oscillating foil," in *Proc. 1996 Symp. Aut. Underwater Veh. Tech.*, 1996, pp. 1–9.

[9] K. Morgansen, V. Duindam, R. Mason, J. Burdick, and R. Murray, "Nonlinear control methods for planar carangiform robot fish locomotion," in *Proc. IEEE Int. Conf. Rob. Aut.*, 2001.

[10] P. Vela, K. Morgansen, and J. Burdick, "Second order averaging methods for oscillatory control of underactuated mechanical systmes," 2002, to appear in Proceedings of the 2002 American Control Conference.

[11] S. Saimek and P. Li, "Motion planning and control of a swimming machine," in *Proc. Amer. Contr. Conf.*, 2001, pp. 125–30.

[12] R. Mason and J. Burdick, "Propulsion and control of deformable bodies in an ideal fluid," in *Proc. IEEE Int. Conf. Rob. Aut.*, 1999, pp. 773–80.

[13] S. Kelly, R. Mason, C. Anhalt, R. Murray, and J. Burdick, "Modelling and experimental investigation of carangiform locomotion for control," in *Proc. Amer. Contr. Conf.*, 1998, pp. 1271–6.

[14] J. Liu, I. Dukes, R. Knight, and H. Hu, "Development of fish-like swimming behaviours for an autonomous robotic fish," in *Proceedings of the Control'04*. University of Bath, England: IEE, September 2004, ID217.

[15] J. Yu, S. Wang, and M. Tan, "A simplified propulsive model of biomimetic robot fish and its realization," *Robotica*, vol. 23, pp. 101–107, 2005.